

**The following resources related to this article are available online at  
[www.sciencemag.org](http://www.sciencemag.org) (this information is current as of December 26, 2009 ):**

**Updated information and services**, including high-resolution figures, can be found in the online version of this article at:

<http://www.sciencemag.org/cgi/content/full/309/5731/121>

**Supporting Online Material** can be found at:

<http://www.sciencemag.org/cgi/content/full/309/5731/121/DC1>

A list of selected additional articles on the Science Web sites **related to this article** can be found at:

<http://www.sciencemag.org/cgi/content/full/309/5731/121#related-content>

This article **cites 27 articles**, 7 of which can be accessed for free:

<http://www.sciencemag.org/cgi/content/full/309/5731/121#otherarticles>

This article has been **cited by** 59 article(s) on the ISI Web of Science.

This article has been **cited by** 2 articles hosted by HighWire Press; see:

<http://www.sciencemag.org/cgi/content/full/309/5731/121#otherarticles>

This article appears in the following **subject collections**:

Cell Biology

[http://www.sciencemag.org/cgi/collection/cell\\_biol](http://www.sciencemag.org/cgi/collection/cell_biol)

Information about obtaining **reprints** of this article or about obtaining **permission to reproduce this article** in whole or in part can be found at:

<http://www.sciencemag.org/about/permissions.dtl>

when seasonality is accounted for, reasonable local temperature estimates can be drawn from the GRIP isotopic record; the correction due to source temperature changes is of lesser importance at glacial-interglacial scales than during rapid events. Moreover, the comparison between our estimate of  $\Delta T_{\text{source}}$  and available North Atlantic sediment-based SST reconstructions suggests that large changes in geographical moisture source location occur both at the orbital and millennial scales. We show that  $\Delta T_{\text{source}}$  reflects obliquity changes and that  $\Delta T_{\text{source}}$  and  $\Delta T_{\text{site}}$  are of opposite sign, both at orbital and millennial time scales. The influence of obliquity on deuterium excess and moisture origin, already identified for Antarctica, is confirmed for Greenland. When cold conditions prevail in the mid- and high latitudes, the moisture origin shifts to milder southward locations (5). Finally, we point to striking similarities between the calcium-dust records and the site-to-source temperature gradient; both are strongly modulated by obliquity, and the coupled climate model results suggest that obliquity could be linked with dust source areas through the land-sea temperature contrast. At the millennial time scale, the site-to-source temperature fluctuations highlight large-scale changes in atmospheric circulation, which is consistent with the observation of simultaneous rapid climate changes at polar, temperate, and tropical latitudes (40) also recorded in Greenland ice chemistry and methane fluctuations (41). Modeling studies have indeed shown that Northern Hemisphere storm tracks are influenced not only by the topography of the ice sheets but also by the sea-ice extent and the meridional temperature gradients (30).

Such large changes in the atmospheric hydrological cycle and associated climate feedbacks are not fully represented in the intermediate-complexity climate models commonly used to understand the mechanisms of abrupt events. Nonetheless, they could play a key role in the generation of instabilities of the ice sheets and the ocean circulation, amplified by changes in sea-ice extent, as has been suggested for the last glacial inception (42).

#### References and Notes

- J. Jouzel *et al.*, *Nature* **329**, 403 (1987).
- W. Dansgaard *et al.*, *Nature* **364**, 218 (1993).
- W. Dansgaard, *Tellus* **16**, 436 (1964).
- C. Lorius, L. Merlivat, in *Isotopes and Impurities in Snow and Ice: Proceedings of the Grenoble Symposium Aug./Sep. 1975* (International Association of Hydrological Sciences, Vienna, 1977), pp. 125–137.
- S. Johnsen, W. Dansgaard, J. White, *Tellus* **41B**, 452 (1989).
- S. J. Johnsen, D. Dahl-Jensen, W. Dansgaard, N. Gundestrup, *Tellus* **47B**, 624 (1995).
- K. M. Cuffey *et al.*, *Science* **270**, 455 (1995).
- D. Dahl-Jensen *et al.*, *Science* **282**, 268 (1998).
- J. Severinghaus, T. Sowers, E. J. Brook, R. B. Alley, M. Bender, *Nature* **391**, 141 (1998).
- J. P. Severinghaus, E. Brook, *Science* **286**, 930 (1999).
- C. Lang, M. Leuenberger, J. Schwander, J. Johnsen, *Science* (1999).
- A. Landais *et al.*, *Earth Planet. Sci. Lett.* **225**, 221 (2004).

- A. Landais *et al.*, *Geophys. Res. Lett.* **31**, L22211 (2004).
- E. A. Boyle, *Geophys. Res. Lett.* **24**, 273 (1997).
- G. Krinner, C. Genthon, J. Jouzel, *Geophys. Res. Lett.* **24**, 2825 (1997).
- M. Werner, U. Mikolajewicz, M. Heimann, G. Hoffmann, *Geophys. Res. Lett.* **27**, 723 (2000).
- J. Jouzel *et al.*, paper presented at the meeting of the European Geophysical Society, Nice, France, 6 to 11 April 2003.
- A. Landais *et al.*, *J. Geophys. Res.* **108**, D06103 (2004).
- A. Armengaud, R. D. Koster, J. Jouzel, P. Ciais, *J. Geophys. Res.* **103**, 8947 (1998).
- V. Masson-Delmotte *et al.*, *J. Geophys. Res.*, in press.
- See supporting data on Science Online.
- V. Masson-Delmotte, B. Stenni, J. Jouzel, *Holocene* **14**, 145 (2004).
- P. Ciais, J. Jouzel, *J. Geophys. Res.* **99**, 16793 (1994).
- B. Stenni *et al.*, *Science* **293**, 2074 (2001).
- K. M. Cuffey, F. Vimeux, *Nature* **412**, 523 (2001).
- F. Vimeux, K. Cuffey, J. Jouzel, *Earth Planet. Sci. Lett.* **203**, 829 (2002).
- G. Hoffmann, J. Jouzel, S. J. Johnsen, *J. Geophys. Res.* **106**, 14265 (2001).
- C. A. Shuman *et al.*, *J. Geophys. Res.* **100**, 9165 (1995).
- G. Hoffmann, M. Stievenard, J. Jouzel, J. W. C. White, S. J. Johnsen, in *Isotope Techniques in the Study of Environmental Changes* (International Atomic Energy Agency, Vienna, 1998), pp. 591–602.
- M. Kageyama, P. J. Valdes, *Geophys. Res. Lett.* **27**, 1515 (2000).
- C. Waelbroeck *et al.*, *Quat. Sci. Rev.* **21**, 295 (2002).
- K. M. Cuffey, G. D. Clow, *J. Geophys. Res.* **102**, 26383 (1997).
- Z. Liu, E. Brady, J. Lynch-Stieglitz, *Paleoceanography* **18**, 10.1029/2002PA000819 (2003).
- E. Cortijo *et al.*, *Paleoceanography* **14**, 23 (1999).
- M. F. Loutre, D. Paillard, F. Vimeux, E. Cortijo, *Earth Planet. Sci. Lett.* **221**, 1 (2004).
- E. Cortijo, L. D. Labeyrie, M. Elliot, E. Balbon, N. Tisnerat, *Quat. Sci. Rev.* **19**, 227 (2000).
- CLIMAP, in *GSA Map and Chart Series, MC-36* (Geological Society of America, Boulder, CO, 1981).
- E. Cortijo *et al.*, *Earth Planet. Sci. Lett.* **146**, 29 (1997).
- K. Fuhrer, E. W. Wolff, S. J. Johnsen, *J. Geophys. Res.* **104**, 31043 (1999).
- L. C. Peterson, G. H. Haug, K. A. Hughen, U. Röhl, *Science* **290**, 1947 (2000).
- J. Chappellaz *et al.*, *Nature* **366**, 443 (1993).
- North Greenland Ice Core Project Members, *Nature* **431**, 147 (2004).
- A. Berger, *Celest. Mech.* **15**, 53 (1977).
- A. M. Grachev, J. P. Severinghaus, *J. Phys. Chem.* **107**, 4636 (2003).
- This work is a contribution to the Greenland Ice Core Project (GRIP) organized by the European Science Foundation. We thank the GRIP scientists, logistics support, and core processors. We also thank the science foundations in Belgium, Denmark, France, Germany, Iceland, Italy, Switzerland, and the UK as well as the EC program. LSCE  $\delta D$  analyses were funded by CEA and Programme National d'Etude de la Dynamique du Climat. We thank E. Cortijo, U. von Grafenstein, F. Vimeux, M. Kageyama, and two anonymous reviewers for discussions on the method and suggestions to improve the manuscript.

#### Supporting Online Material

www.sciencemag.org/cgi/content/full/309/5731/118/DC1  
Materials and Methods  
Table S1

10 December 2004; accepted 20 May 2005  
10.1126/science.1108575

## A Magnetic Nanoprobe Technology for Detecting Molecular Interactions in Live Cells

Jaejoon Won,<sup>1</sup> Mina Kim,<sup>1</sup> Yong-Weon Yi,<sup>1</sup> Young Ho Kim,<sup>2</sup> Neoncheol Jung,<sup>2</sup> Tae Kook Kim<sup>1\*</sup>

Technologies to assess the molecular targets of biomolecules in living cells are lacking. We have developed a technology called magnetism-based interaction capture (MAGIC) that identifies molecular targets on the basis of induced movement of superparamagnetic nanoparticles inside living cells. Efficient intracellular uptake of superparamagnetic nanoparticles (coated with a small molecule of interest) was mediated by a transducible fusogenic peptide. These nanoprobes captured the small molecule's labeled target protein and were translocated in a direction specified by the magnetic field. Use of MAGIC in genome-wide expression screening identified multiple protein targets of a drug. MAGIC was also used to monitor signal-dependent modification and multiple interactions of proteins.

Modern medicine faces the challenge of developing safer and more effective therapies. However, many drugs currently in use were identified without knowledge of their molecular targets (1, 2). Bioactive natural products are an important source of drug leads, but

their modes of action are usually unknown (2). Elucidation of their physiological targets is essential for understanding their therapeutic and adverse effects, thereby enabling the development of second-generation therapeutics. Moreover, the discovery of novel targets of clinically proven compounds may suggest new therapeutic applications (3). Target identification (ID) is also important in chemical biology, where high-throughput screening is used to identify small molecules with a desired phenotype (4, 5). Despite the great benefits of such

<sup>1</sup>Department of Biological Sciences, Korea Advanced Institute of Science and Technology, Daejeon 305-701, Korea. <sup>2</sup>CGK Co. Ltd., Daejeon 305-701, Korea.

\*To whom correspondence should be addressed. E-mail: tkkim@kaist.ac.kr

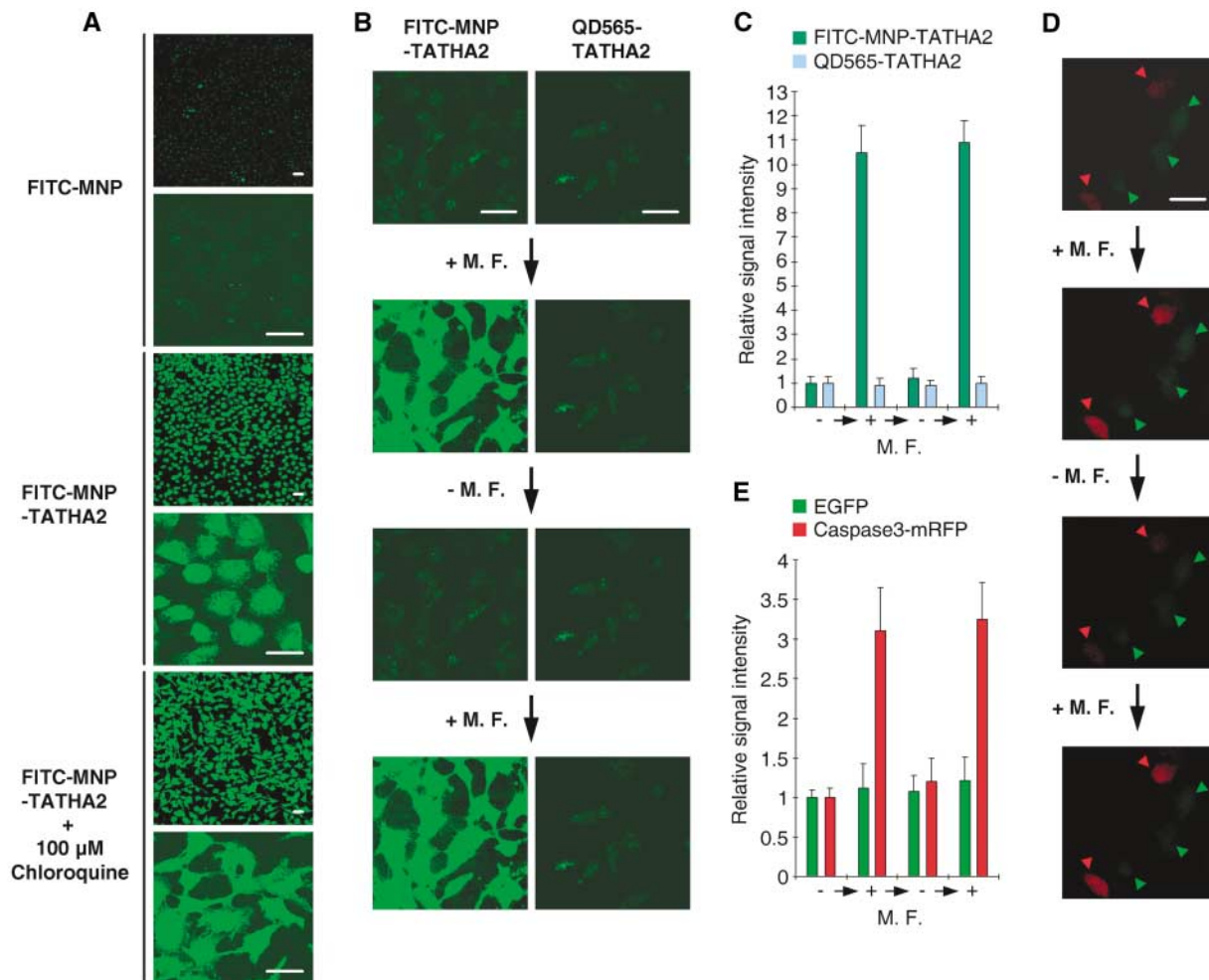


**Fig. 1.** Proof-of-principle experiments for MAGIC. (A) Enhanced intracellular uptake and endosomal escape of MNPs by TAT-HA2. HeLa cells were incubated with MNP coated with FITC (FITC-MNP) or with FITC and TAT-HA2 (FITC-MNP-TATHA2) in the absence or presence of 100  $\mu$ M chloroquine for 12 hours. Live-cell confocal images were taken to show the intracellular distribution of FITC-labeled MNPs. Scale bars, 50  $\mu$ m. (B and C) Translocation of MNPs inside cells by the magnetic field. HeLa cells were incubated with FITC-MNP-TATHA2 or QD565-TATHA2 in the presence of 100  $\mu$ M chloroquine for 12 hours. Scale bars in (B), 50  $\mu$ m. (D and E) DEVD-coated MNPs direct the translocation of caspase-3-

mRFP by the magnetic field. HeLa cells were transfected with the expression plasmids for caspase-3-mRFP or EGFP, detached, mixed together, and replated. These cells were incubated with MNPs coated with DEVD and TAT-HA2 in the presence of 100  $\mu$ M chloroquine for 12 hours. In (B) and (D), live-cell confocal images were taken before and after application of a magnetic field (M.F.), with the focal plane at the cellular basal surface. Cells expressing EGFP or caspase-3-mRFP are indicated by green or red arrowheads, respectively, in (D). Scale bar in (D), 50  $\mu$ m. In (C) and (E), quantitative analysis of the signals was performed with more than 100 cells.

a screen, this approach has been hampered by the daunting task of target ID (1, 4, 5).

Superparamagnetic nanoparticles (MNPs) are biocompatible and are in routine clinical use (6, 7). We built on these nanomagnetic probes to develop a target ID technology MAGIC, to directly probe molecular interactions inside living cells with high sensitivity and selectivity (fig. S1). Streptavidin-conjugated MNPs were used as a generic reagent to attach biotinylated molecules to the nanoprobe. After internalization of small molecule-coated MNPs into the cells, protein(s) bind to the small molecule on the MNP. Thus, when a magnetic field is applied, the MNP and associated target protein(s) can be concentrated. Fusion of a fluorescent probe to the target protein renders this translocation easily detectable by confocal microscopy.

To visualize and track the distribution of MNPs within cells, we labeled MNPs with fluorescein isothiocyanate (FITC) (8) (Fig. 1A). FITC-MNPs were not efficiently introduced into the cell cytosol. Most of the internalized FITC-MNPs appeared to be trapped within endocytic vesicles (Fig. 1A). Attachment of transducible fusogenic TAT-HA2 peptide on the MNPs markedly enhanced endocytic uptake and subsequent release from endosomes. It is currently understood that the high density of cationic residues in the protein transduction domain of human immunodeficiency virus TAT protein causes an electrostatic interaction with the negatively charged cell surface, thus enhancing the chance of endocytic internalization, whereas the N-terminal 20 amino acids of the influenza virus hemagglutinin protein HA2 desta-

bilizes endosomal membranes, causing them to release their contents into the cytosol (9, 10). Cotreatment with chloroquine, which is known to enhance endosome disruption (11), further increased the concentration of MNPs outside endosomes (Fig. 1A).

We next addressed whether internalized MNPs could be moved inside cells by an external magnetic field (Fig. 1, B and C). HeLa cells were transfected with MNPs coated with FITC and TAT-HA2. As a control, a luminescent nanocrystal quantum dot, QD565, which does not exhibit magnetism (12), was internalized into another set of HeLa cells with the use of TAT-HA2. Specific translocation of MNPs, but not QD565, was observed inside cells after brief application of a magnetic field (Fig. 1, B and C). Furthermore, this translocation was reversible; the

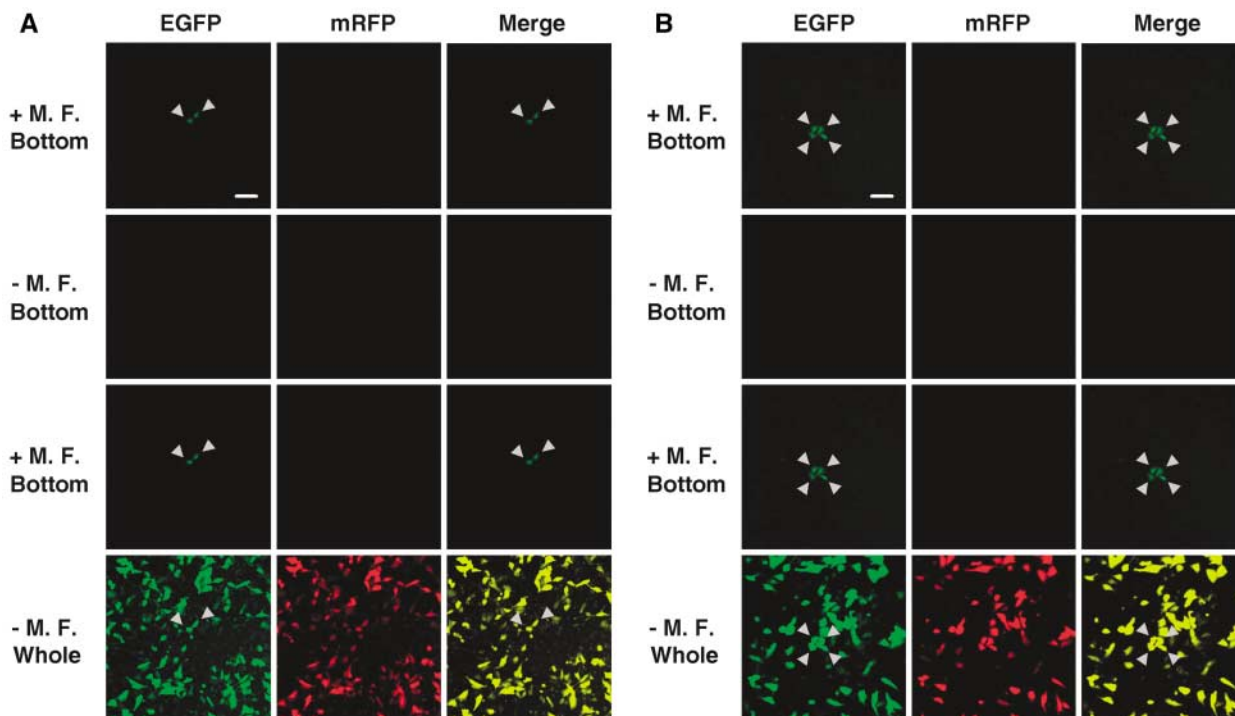


**Fig. 2.** Molecular target ID based on MAGIC. (A and B) HeLa cells were infected with the retroviral EGFP–fusion protein expression library (fig. S2B). After incubation of these cells with MNPs coated with FK506 and TAT-HA2 in the presence of 100 μM chloroquine for 12 hours, the subcellular localization of EGFP was examined in the absence or presence of a magnetic field (M.F.). To address potential false positives, we simultaneously monitored mRFP

bicistronically coexpressed with EGFP–fusion protein. Live-cell confocal images were taken with the focal plane at the cellular basal surface (bottom) or with the pinhole size increased to collect whole-cell images (whole). Arrowheads indicate positive clones. RT-PCR and sequence analysis of mRNAs from these clones identified several proteins (Table 1) including FKBP12 (A) and an unknown protein with NCBI accession number BAB15266 (B). Scale bars, 100 μm.

**Table 1.** Protein targets of FK506 identified from expression cloning with the use of MAGIC. A total of 19 positive clones were identified from ~10<sup>7</sup> cells. The number of independent cDNA clones for each protein isolated from the screen is shown.

NCBI accession number	Protein name	Number isolated	Reported binding to FK506
NP_463460	FKBP12	4	Yes (14–17)
Q16645	FKBP12.6	2	Yes (17)
P26885	FKBP13	1	Yes (17)
AAA58475	FKBP25	2	Yes (15, 17)
Q02790	FKBP52	3	Yes (16, 17)
AAA86245	FKBP54	2	Yes (17)
NP_068758	FKBP65	1	Yes (17)
BAB15266	Unnamed	1	No
BAB15220	Unnamed	1	No
BAC03954	Unnamed	1	No
BAD18781	Unnamed	1	No
Total		19	

MNPs rapidly diffused away upon removal of the magnetic field and were redirected when it was reapplied.

We determined whether the MAGIC principle could be used to detect the intracellular target for Asp-Glu-Val-Asp (DEVD), an apoptosis inhibitor known to bind caspase-3 (13) (Fig. 1, D and E). HeLa cells were transfected with the expression construct for enhanced green fluorescent protein (EGFP) or caspase-3 fused to monomeric red fluorescent protein (mRFP). Next, these two sets of transfectants were detached, mixed, and replated

for incubation with MNPs coated with DEVD and TAT-HA2. A notable amount of “red” signal, but not “green” signal, was translocated in the direction of the magnetic field (Fig. 1, D and E), indicating a specific interaction between DEVD and caspase-3 inside cells. This translocation was reversible upon removal and reapplication of the magnetic field (Fig. 1, D and E) (movie S1).

To use MAGIC in systematic target ID for a bioactive small molecule, we exploited expression cloning based on a retroviral EGFP fusion protein expression library (Fig. 2). We

sought to identify the receptor(s) for an immunosuppressant, FK506 (fig. S2A), in a genome-wide screen. A normalized EGFP-tagged cDNA library was generated (8); cDNAs from multiple human tissues were fused to the 5′ or 3′ end of the gene encoding EGFP, and mRFP was coexpressed as an internal control to address potential false positives (fig. S2B). This library was stably expressed in HeLa cells by retroviral transduction. After introduction of FK506-coated MNPs into these cells, a magnetic field was applied, and the subcellular localization of proteins expressed from cDNA-EGFP fusions was examined. Nineteen positive clones were identified that exhibited specific translocation of EGFP in the direction of the magnetic field while the subcellular localization of mRFP remained unchanged (Table 1 and Fig. 2). Reverse transcription polymerase chain reaction (RT-PCR) and BLAST analysis of mRNAs from these clones identified overlapping transcripts of several known FK506-binding proteins and proteins of unknown function (Table 1 and Fig. 2) (14–17). Specific interaction of these proteins with FK506 was verified by competition analysis (fig. S3). These interactions were also readily detected with other cell types (fig. S4).

The specificity of these interactions could be distinguished readily from background and

false positive signals on the basis of reversible translocation manipulated by magnetic field at the initial screening stage (Fig. 2). Overall, the screen identified diverse targets with high efficiency and no false positives (Table 1). The additional targets discovered for FK506 might give some clues about the molecular mechanisms underlying its unexpected therapeutic actions and debilitating side effects (17).

To evaluate the feasibility of MAGIC for probing intracellular signaling processes, we used the NF- $\kappa$ B/I $\kappa$ B pathway (Fig. 3). Members of the NF- $\kappa$ B family (e.g., RelA/p65) are sequestered in the cytoplasm by I $\kappa$ B family members (e.g., I $\kappa$ B $\alpha$ ). Various stimuli, including proinflammatory cytokines such as tumor necrosis factor- $\alpha$  (TNF- $\alpha$ ), induce the phosphorylation of I $\kappa$ B $\alpha$  on two serine residues, Ser<sup>32</sup> and Ser<sup>36</sup> (18). This phosphorylation results in recognition of I $\kappa$ B $\alpha$  by the F box protein  $\beta$ TrCP of the SKP1/cullin/F-box ubiquitin ligase complex, leading to ubiquitin-dependent proteolysis of I $\kappa$ B $\alpha$ . These regulated protein-protein interactions allow NF- $\kappa$ B proteins to translocate into the nucleus, resulting in the expression of target genes.

We first tested whether signal-induced protein phosphorylation could be detected

with MAGIC (Fig. 3, A to D). After expression of I $\kappa$ B $\alpha$  fused to mRFP in HeLa cells, these cells were loaded with MNPs triple-labeled with TAT-HA2, FITC, and antibody to phosphorylated Ser<sup>32</sup> of I $\kappa$ B $\alpha$  (8). Before stimulation, translocation of I $\kappa$ B $\alpha$ -mRFP was barely detectable, despite active accumulation of FITC signal in the direction of the magnetic field (Fig. 3, B to D). In contrast, brief stimulation with TNF- $\alpha$  markedly induced the magnetic field-directed translocation of mRFP signal for I $\kappa$ B $\alpha$ , faithfully reflecting the phosphorylation of I $\kappa$ B $\alpha$  in response to TNF- $\alpha$  inside cells (fig. S5). Under these conditions, SC-514, an inhibitor of I $\kappa$ B kinase (IKK), prevented TNF- $\alpha$ -induced translocation of I $\kappa$ B $\alpha$ -mRFP (Fig. 3, C and D), further emphasizing the specificity of the method.

Next we examined whether signal-dependent protein-protein interactions could be detected with MAGIC (Fig. 3, A, E to G). To entrap I $\kappa$ B $\alpha$  with MNPs inside cells, we used MNPs coated with FK506 and TAT-HA2 (TATHA2-MNP-FK506) together with I $\kappa$ B $\alpha$  tagged with FK506-binding protein, FKBP12 (I $\kappa$ B $\alpha$ -ECFP-FKBP12; Fig. 3, A, E to G). After expression of I $\kappa$ B $\alpha$ -ECFP-FKBP12, EYFP-RelA, and

mRFP- $\beta$ TrCP in HeLa cells, these cells were transfected with TATHA2-MNP-FK506. Application of a magnetic field directed the translocation of ECFP signal (Fig. 3F), reflecting I $\kappa$ B $\alpha$  recruitment around MNPs by FK506-FKBP12 interaction inside cells. Under these conditions, EYFP-RelA, but not mRFP- $\beta$ TrCP, was directed toward the magnetic field, indicating that interaction occurs between I $\kappa$ B $\alpha$  and RelA, but not between I $\kappa$ B $\alpha$  and  $\beta$ TrCP. Upon stimulation with TNF- $\alpha$ , a marked increase in mRFP- $\beta$ TrCP translocation was observed (Fig. 3, F and G), demonstrating signal-induced interaction between I $\kappa$ B $\alpha$  and  $\beta$ TrCP. Notably, SC-514 blocked TNF- $\alpha$ -induced translocation of mRFP- $\beta$ TrCP (Fig. 3, F and G). Thus, MAGIC can faithfully probe molecular interactions dynamically regulated by specific signals in live cells.

In certain disease conditions (e.g., systemic inflammation), several cellular functions, such as endocytosis, are known to be compromised (19, 20). To demonstrate MAGIC in cells impaired in endocytosis, we adopted microinjection that can introduce exogenous materials directly into cells without passing through endocytic vesicles (21) (fig. S6). The signal-induced phosphorylation and protein-protein

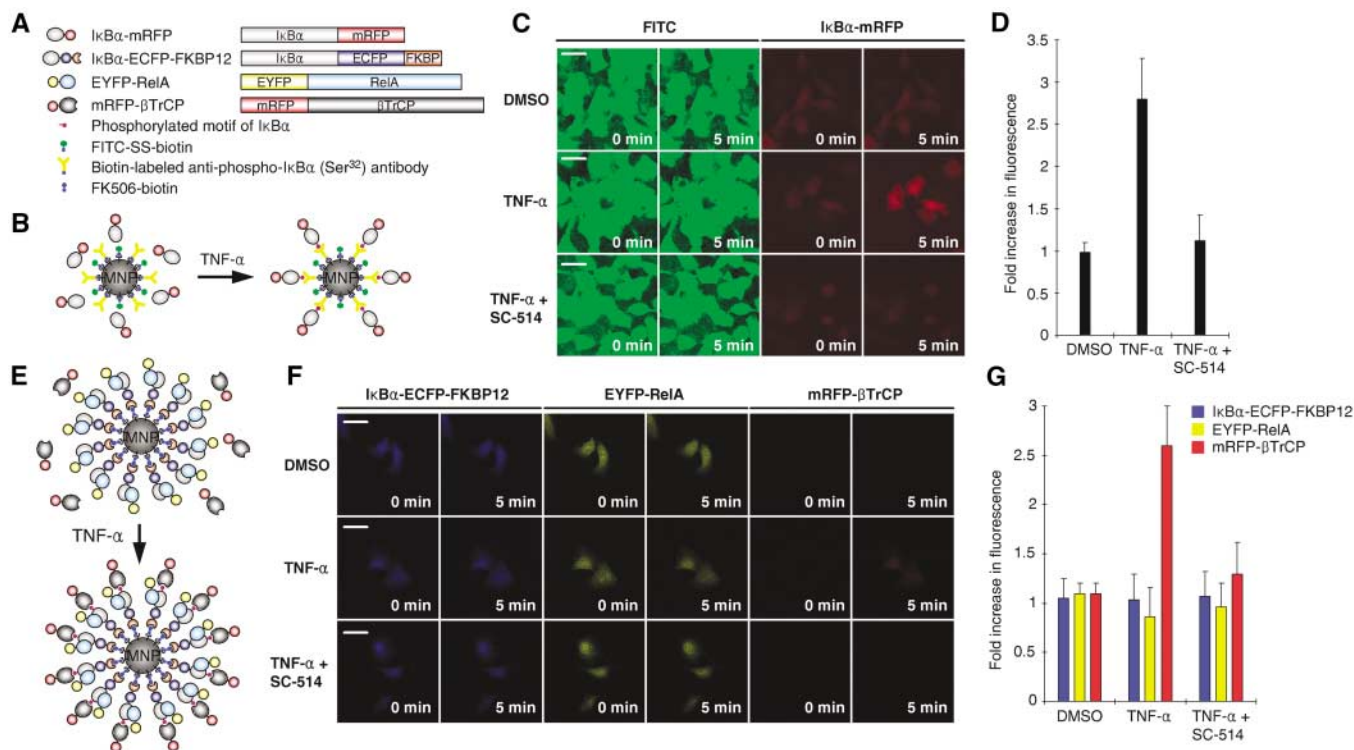


**Fig. 3.** Monitoring biological signaling processes by MAGIC. (A) Schematic of I $\kappa$ B $\alpha$ -mRFP, I $\kappa$ B $\alpha$ -ECFP-FKBP12, EYFP-RelA, and mRFP- $\beta$ TrCP. Symbols used in (B) and (E) are also explained. (B to D) Detection of signal-induced phosphorylation of I $\kappa$ B $\alpha$ . After transfection of HeLa cells with the expression plasmid for I $\kappa$ B $\alpha$ -mRFP, MNPs coated with antibody to phosphorylated Ser<sup>32</sup> of I $\kappa$ B $\alpha$ , FITC, and TAT-HA2 were introduced into these cells. Magnetic field-induced translocation of FITC and mRFP signals was monitored before and after stimulation with TNF- $\alpha$  (10 ng/ml) for 5 min in the absence or presence of prior treatment with SC-514 (1 mM). (E to G) Detection of signal-

dependent association of I $\kappa$ B $\alpha$  with  $\beta$ TrCP. After transfection of HeLa cells with the expression plasmids for I $\kappa$ B $\alpha$ -ECFP-FKBP12, EYFP-RelA, and mRFP- $\beta$ TrCP, MNPs coated with FK506 and TAT-HA2 were introduced into these cells. Magnetic field-induced translocation of enhanced cyan fluorescent protein (ECFP), enhanced yellow fluorescent protein (EYFP), and mRFP signals was monitored before and after stimulation with TNF- $\alpha$  (10 ng/ml) for 5 min in the absence or presence of prior treatment of SC-514 (1 mM). Scale bars, 50  $\mu$ m. Shown in (D) and (G) are quantitative analyses of induced signals after stimulation with TNF- $\alpha$  for 5 min with more than 100 cells.

interaction between I $\kappa$ B $\alpha$  and RelA were probed in HeLa cells pretreated with TNF- $\alpha$ , which inhibited the endocytic uptake of MNPs, as described (20). MNPs coated with antibody to phosphorylated Ser<sup>32</sup> of I $\kappa$ B $\alpha$  or with FK506 were microinjected into TNF- $\alpha$ -pretreated HeLa cells expressing I $\kappa$ B $\alpha$ -mRFP or I $\kappa$ B $\alpha$ -ECFP-FKBP12/EYFP-RelA/mRFP- $\beta$ TrCP, respectively (8). Signal-induced phosphorylation and interaction of the NF- $\kappa$ B/I $\kappa$ B pathway were readily detected by MAGIC in this experimental setting (fig. S6).

MAGIC offers several advantages over target ID methods currently in use. First, it directly translates a physical molecular interaction into a clear readout signal, unlike indirect readout methods that are dependent on intermediary interactions (22), overall expression profiles (23), or complex biological phenotypes (24). Thus, intrinsic false positives/negatives or error-prone deductions about molecular target(s) of a small molecule are obviated. Second, by probing such interactions in a physiologically relevant context, misleading outcomes produced by an artificial experimental setting (22, 24–28) can be greatly diminished. Third, it is amenable to dynamic, single-cell analysis of interactions. Finally, MAGIC can be used to detect a variety of biological interactions and protein modifications

within live cells in a broad range of tissues and disease states. With the great advantage of being able to detect dynamic interactions between the biomolecules within mammalian cells, this technology could be exploited in genome-wide interaction screens.

The benefits of MAGIC may be best achieved through efficient and nondisruptive introduction of MNPs into cells. Prolonged incubation of cells with TAT-HA2-conjugated MNPs may affect cellular physiology, and microinjection cannot be used for large populations of cells. Other technologies for delivering biologically active cargos into cells (10) will be helpful to complement MAGIC.

#### References and Notes

1. L. Burdine, T. Kodadek, *Chem. Biol.* **11**, 593 (2004).
2. J. Clardy, C. Walsh, *Nature* **432**, 829 (2004).
3. T. T. Ashburn, K. B. Thor, *Nat. Rev. Drug Discov.* **3**, 673 (2004).
4. R. L. Strausberg, S. L. Schreiber, *Science* **300**, 294 (2003).
5. B. R. Stockwell, *Nature* **432**, 846 (2004).
6. M. Lewin *et al.*, *Nat. Biotechnol.* **18**, 410 (2000).
7. C. Alexiou *et al.*, *Cancer Res.* **60**, 6641 (2000).
8. See supporting data on Science Online.
9. J. S. Wadia, R. V. Stan, S. F. Dowdy, *Nat. Med.* **10**, 310 (2004).
10. A. Joliot, A. Prochiantz, *Nat. Cell Biol.* **6**, 189 (2004).
11. N. J. Caron, S. P. Quenneville, J. P. Tremblay, *Biochem. Biophys. Res. Commun.* **319**, 12 (2004).
12. X. Michalet *et al.*, *Science* **307**, 538 (2005).

13. A. Mack, C. Fürmann, G. Häcker, *J. Immunol. Methods* **241**, 19 (2000).
14. M. W. Harding, A. Galat, D. E. Uehling, S. L. Schreiber, *Nature* **341**, 758 (1989).
15. Y.-J. Jin, S. J. Burakoff, B. E. Bierer, *J. Biol. Chem.* **267**, 10942 (1992).
16. D. A. Peattie *et al.*, *Proc. Natl. Acad. Sci. U.S.A.* **89**, 10974 (1992).
17. J. O. Liu, *Biochem. Biophys. Res. Commun.* **311**, 1103 (2003).
18. M. Karin, Y. Yamamoto, Q. M. Wang, *Nat. Rev. Drug Discov.* **3**, 17 (2004).
19. M. González-Gaitán, H. Stenmark, *Cell* **115**, 513 (2003).
20. J. E. Baatz, Y. Zou, T. R. Korfhagen, *Biochim. Biophys. Acta* **1535**, 100 (2001).
21. A. M. Derfus, W. C. W. Chan, S. N. Bhatia, *Adv. Mater.* **16**, 961 (2004).
22. E. J. Licitra, J. O. Liu, *Proc. Natl. Acad. Sci. U.S.A.* **93**, 12817 (1996).
23. M. J. Marton *et al.*, *Nat. Med.* **4**, 1293 (1998).
24. P. Y. Lum *et al.*, *Cell* **116**, 121 (2004).
25. Y. Oda *et al.*, *Anal. Chem.* **75**, 2159 (2003).
26. P. P. Sche, K. M. McKenzie, J. D. White, D. J. Austin, *Chem. Biol.* **6**, 707 (1999).
27. G. MacBeath, S. L. Schreiber, *Science* **289**, 1760 (2000).
28. F. G. Kuruvilla *et al.*, *Nature* **416**, 653 (2002).
29. We thank C. O. Joe, R. Y. Tsien, J. Choe, P. M. Howley, J. Campisi, J. A. Schmid, and G. P. Nolan for reagents. Supported by CGK Co. Ltd.

#### Supporting Online Material

www.sciencemag.org/cgi/content/full/309/5731/1217/DC1

Materials and Methods

Figs. S1 to S6

Movie S1

References and Notes

29 March 2005; accepted 9 May 2005  
10.1126/science.1112869

## Cell-to-Cell Transfer of Bacterial Outer Membrane Lipoproteins

Eric Nudleman,\* Daniel Wall,† Dale Kaiser‡

*Myxococcus xanthus* cells can glide forward by retracting type IV pili. Tgl, an outer membrane lipoprotein, is necessary to assemble pili. Tgl mutants can be transiently “stimulated” if brought into end-to-end contact with *tgl*<sup>+</sup> donor cells. By separating the stimulated recipient cells from donor cells, we found that Tgl protein was transferred from the donors to the rescued recipient cells. Mutants lacking CglB lipoprotein, which is part of a second gliding engine, could also be stimulated, and CglB protein was transferred from donor to recipient cells. The high transfer efficiency of Tgl and CglB proteins suggests that donor and recipient cells briefly fuse their outer membranes.

Myxobacteria move by gliding on surfaces—an effective mode of translocation in their soil habitat (1). *Myxococcus xanthus* moves smoothly in the direction of its long axis, then reverses and moves in the opposite direction. It has no flagella and cannot swim; its gliding is propelled by two polar engines that

are encoded by the A and the S genes (2). The A engines appear to extrude polymer chains from the trailing ends of cells, which gelate, pushing the cells forward (3). Slime is extruded from the trailing end only (4). The S genes encode hairlike appendages projecting from the leading end of the cell—the type IV pili (5, 6)—and they pull a cell forward by retracting (7). Many proteobacterial pathogens have type IV pili (8). *M. xanthus* type IV pili are polar (6), and S motility is limited to cells within pilus-contact distance of each other (9).

A common set of 10 proteins is necessary for the assembly and retraction of type IV pili in *M. xanthus*, *Pseudomonas aeruginosa*, and *Neisseria gonorrhoeae* (8). One of those proteins, known as PilA in *M. xanthus*, con-

stitutes the pilus filament, a helical array of PilA monomers (10). The filament is thought to pass through the outer membrane within a gated channel formed by the PilQ secretin protein (11). Secretins are multimeric channels large enough to pass folded proteins (12). Secretins often have cognate lipoproteins that facilitate their assembly in the outer membrane (13, 14).

The Tgl lipoprotein is necessary to assemble a detergent-resistant PilQ secretin in *M. xanthus* (15). Nevertheless, *tgl* mutants can be stimulated to assemble pili and to glide after transient contact with *tgl*<sup>+</sup> donor cells (16, 17). Cells with a *tgl* mutation lack S motility but have normal A motility. Tgl stimulation specifically restores their S motility (2). To render stimulation visible by its effect on motility, we transferred a mutant *tgl* locus into an A<sup>−</sup> background, creating a nonmotile strain. Strain DK8602 (table S1) lacked both A and S motility and formed a smooth-edged colony (Fig. 1A). When DK8602 was mixed with a nonmotile *tgl*<sup>+</sup> donor strain ( $\Delta$ *pilA*, *aglB1*), the mixed population initially had a smooth colony edge reflecting both strains’ lack of A and S motility (Fig. 1A). Recipient cells swarm beyond the original colony edge as flares when they are stimulated (Fig. 1B), which shows that the cells had assembled retractile pili.

To distinguish donor from recipient cells in a Tgl-stimulation mixture, we expressed the green fluorescent protein (GFP) in one population or the other. When the recipient strain

Departments of Developmental Biology and Biochemistry, Stanford University School of Medicine, 8300 Beckman Center, 279 Campus Drive, Stanford, CA 94305, USA.

\*Present address: Albert Einstein College of Medicine, 1300 Morris Park Avenue, Bronx, NY 10461, USA.

†Present address: Anadys Pharmaceuticals, 3115 Merryfield Row, San Diego, CA 92121, USA.

‡To whom correspondence should be addressed. E-mail: kaiser@cmgm.stanford.edu

# RETRACTION

Post date 24 April 2009

*Science* has received the results of the KAIST Research Integrity Committee investigation of the Report published in *Science* by J. Won *et al.* (1). According to an English translation commissioned by *Science*, the committee found that the original data underlying the experiments reported in *Science* are not available and that many of the results in the paper were fabricated. Therefore, the data, results, and conclusions in the Won *et al.* Report are clearly not reliable, and *Science* is hereby retracting the paper.

Bruce Alberts

**Reference**

1. J. Won *et al.*, *Science* **309**, 121 (2005).